Physiology of afferent neurons in larval zebrafish provides a functional framework for lateral line somatotopy

James C. Liao and Melanie Haehnel

J Neurophysiol 107:2615-2623, 2012. First published 15 February 2012;
doi: 10.1152/jn.01108.2011

J Neurophysiol 107: 2615–2623, 2012.
First published February 15, 2012; doi:10.1152/jn.01108.2011.

Physiology of afferent neurons in larval zebrafish provides a functional framework for lateral line somatotopy

James C. Liao and Melanie Haehnel
The Whitney Laboratory for Marine Bioscience, Department of Biology, University of Florida, St. Augustine, Florida

Submitted 2 December 2011; accepted in final form 14 February 2012

Liao JC, Haehnel M. Physiology of afferent neurons in larval zebrafish provides a functional framework for lateral line somatotopy. *J Neurophysiol* 107: 2615–2623, 2012. First published February 15, 2012; doi:10.1152/jn.01108.2011.—Fishes rely on the neuromasts of their lateral line system to detect water flow during behaviors such as predator avoidance and prey localization. Although the pattern of neuromast development has been a topic of detailed research, we still do not understand the functional consequences of its organization. Previous work has demonstrated somatotopy in the posterior lateral line, whereby afferent neurons that contact more caudal neuromasts project more dorsally in the hindbrain than those that contact more rostral neuromasts (Gompel N, Dambly-Chaudiere C, Ghysen A. *Development* 128: 387–393, 2001). We performed patch-clamp recordings of afferent neurons that contact neuromasts in the posterior lateral line of anesthetized, transgenic larval zebrafish (*Danio rerio*) to show that larger cells are born earlier, have a lower input resistance, a lower spontaneous firing rate, and tend to contact multiple neuromasts located closer to the tail than smaller neurons, which are born later, have a higher input resistance, a higher spontaneous firing rate, and tend to contact single neuromasts. We suggest that early-born neurons are poised to detect large stimuli during the initial stages of development. Later-born neurons are more easily driven to fire and thus likely to be more sensitive to local, weaker flows. Afferent projections onto identified glutamatergic regions in the hindbrain lead us to hypothesize a novel mechanism for lateral line somatotopy. We show that afferent fibers associated with tail neuromasts respond to stronger stimuli and are wired to dorsal hindbrain regions associated with Mauthner-mediated escape responses and fast, avoidance swimming. The ability to process flow stimuli by circumventing higher-order brain centers would ease the task of processing where speed is of critical importance. Our work lays the groundwork to understand how the lateral line translates flow stimuli into appropriate behaviors at the single cell level.

patch-clamp electrophysiology; neuromast; development; swimming; flow sensing

THE LATERAL LINE SYSTEM consists of discrete clusters of hair cells and support cells that together make up the neuromasts, which in adult fishes are either directly exposed on the skin surface (superficial neuromasts) or enclosed in fluid-filled canals just below the skin surface (canal neuromasts). Hair cells transmit information about hydrodynamic stimuli to afferent fibers, which in turn relay information to the hindbrain (Coombs et al. 1998; Liao 2010; McCormick 1989; Montgomery et al. 1996; Nicolson et al. 1998). Detailed behavioral and electrophysiological work in adult fishes has demonstrated that the superficial and canal neuromasts are used to detect flow velocity and acceleration, respectively (Coombs et al. 1989; Dijkgraaf 1963; Engelmann et al. 2002; Montgomery et al. 2000), but we still lack a framework to understand the functional organization of neuromasts. Our ability to decipher how hydrodynamic information is processed would be greatly accelerated if we could monitor afferent connectivity and physiology at the single cell level. This level of resolution is not possible in adult fishes, which, in some species, can possess up to thousands of neuromasts.

Larval zebrafish only have a few dozen neuromasts and afferent neurons. When combined with their optical transparency and the ease in which one can genetically label subsets of neurons with fluorescent proteins, larval zebrafish are emerging as a model system to study the patterning and connectivity of neuromasts and hair cells during development (Alexandre and Ghysen 1999; Faucherre et al. 2009; Ledent 2002; Nagiel et al. 2008; Raible and Kruse 2000; Sarrazin et al. 2010; Sato et al. 2010). For example, somatotopy has been clearly demonstrated, whereby afferent neurons of the posterior lateral line system that contact more caudal neuromasts project more dorsally in the hindbrain than those that contact more rostral neuromasts (Gompel et al. 2001). The tractability of the lateral line at this stage provides a strong opportunity for the next step: to reveal the physiology of individual afferent neurons. Here, we use whole cell patch-clamp recordings to show that an initial, broad sensory scaffold develops to detect strong flows, followed by a subsequent wave of afferent neurons and neuromasts that are poised to detect weaker flows. To understand better the functional consequence of the intrinsic properties of afferent neurons, we looked for potential postsynaptic contacts in a population of hindbrain neurons with known transmitter phenotypes. Recently, glutamatergic neurons in the hindbrain were shown to be organized into stripes that reflect a broad underlying functional patterning (Kinkhabwala et al. 2010; Koyama et al. 2010). We looked to see whether posterior lateral line projections into the hindbrain were integrated into the map of these excitatory neurons, which is linked to sensorymotor behaviors. Our physiological results, which are consistent with lateral line somatotopy, provide an efficient way to separate different types of flow information at the periphery to ease the task of processing inputs at higher-order brain centers (Alexandre and Ghysen 1999; New et al. 1996; Plachta et al. 2003).

METHODS

Fish care. Electrophysiological and imaging experiments were conducted on 5- to 6-day postfertilization (dpf) zebrafish larvae (*Danio rerio*) obtained from a laboratory stock of wild-type and transgenic adults. Two transgenic lines were used, HuC:Kaede larvae, which express a UV light-sensitive photoconvertible protein under the

Address for reprint requests and other correspondence: J. C. Liao, The Whitney Laboratory for Marine Bioscience, Dept. of Biology, Univ. of Florida, 9505 Oceanshore Blvd., St. Augustine, FL 32080 (e-mail: jliao@whitney.ufl.edu).

control of a pan-neuronal promoter (Sato et al. 2006), and Vglut-GFP larvae, which express green fluorescent protein (GFP) driven by the promoter vglut2.1 to mark glutamatergic neurons (Bae et al. 2009). Fish were reared in an in-house laboratory facility at 28.5°C. Experiments were performed at room temperature (~24°C) under the National Institutes of Health guidelines regarding animal experimentation and were approved by the University of Florida's Institutional Animal Care and Use Committee.

Photoconversion. In 5-dpf larvae, there are three distinct populations of neuromasts, derived from two distinct placodes (Sarrazin et al. 2010). Figure 1 shows that placode I develops at 17 h postfertilization (hpf) and gives rise to primordium I and its associated L neuromasts. Placode II develops ~24 hpf and gives rise to primordium II and primordium D, which in turn gives rise to the LII and D neuromasts, respectively. HuC:Kaede larvae still within their chorion were flashed with UV light for 10–20 s at 17 hpf and imaged at 5 dpf. Under this protocol, all afferent neurons that are born before or at 17 hpf are red and considered older than those that are born after 17 hpf, which are green. We used a GFP band pass and a Texas red filter cube (41017 EN GFP C62942 and 41004 TR C127531; Omega Optical) to confirm that all neurons that were green before flashing were converted to red after flashing. Fish were then raised in the dark at 28.5°C in a DigiTherm incubator (Tritech Research). At 5 dpf, afferent neurons were imaged with IPLab v3.7 software controlling an integrating 12-bit mono charge-coupled device (CCD) camera (QImaging) mounted on an upright Olympus BX51WI fixed stage compound microscope fitted with a ×40 Olympus water-immersion lens.

Single-cell electroporation of afferents in the ganglion. Larvae were anesthetized in a 0.02% solution of MS-222 and paralyzed by immersion in 1 mg/ml α-bungarotoxin (Sigma-Aldrich) mixed in 10% Hank's solution. Larvae were positioned by pinning them on their side with etched tungsten pins (0.004-in. diameter; A-M Systems) into a Sylgard-bottomed dish or embedded in 1.4% DNA-grade low-melting-point agar (Fisher Scientific) mixed in extracellular solution (134 mM NaCl, 2.9 mM KCl, 1.2 mM $MgCl_2$, 2.1 mM $CaCl_2$, 10 mM glucose, 10 mM HEPES buffer, adjusted to pH 7.8 with NaOH). Old and young cells were targeted for electroporation under standard Nomarski optics with an Axoporator 800 (Molecular Devices). Pulse protocol was as follows: 5–10 V, ± step square pulse, multiple 100- to 300-ms train pulses, 10- to 20-Hz frequency, and a pulse-width 1–10 ms. Electrodes were pulled from borosilicate glass (inside diameter = 0.86 mm, outside diameter = 1.5 mm; Model G150-F-3; Warner Instruments) on a Model P-97 Flaming/Brown micropipette puller (Sutter Instrument). Electrodes were pulled to 10- to 15-MΩ resistances and filled with 10% Alexa Fluor 647 Dextran (10,000-Da mol mass anionic; Molecular Probes) in 10% Hank's solution. A four-axis micromanipulator (Siskiyou) was used to advance the electrode through the skin and into the ganglion to label individual somata. For some preparations, we first broke the skin with a sentinel electrode placed under constant positive pressure (~5 mmHg) using a pneumatic transducer (Fluke Biomedical) to clear the path for an electroporation electrode to be lowered into the ganglion. Once an afferent somata was labeled, we waited several minutes to ensure dye uptake and then switched to a Cy5 filter set and an epifluorescence light source to follow the projection down the body to confirm the number and location of neuromasts connected to the cell. In some cases, we better visualized afferent terminals at the base of a neuromast by imaging fish on a Leica SP5 confocal microscope.

In vivo whole cell patch recordings in the posterior lateral line ganglion. Whole cell recordings were done in current-clamp mode in wild-type and transgenic 5-dpf larvae, similar to previous studies (Bhatt et al. 2007; Liao 2010; Liao and Fetcho 2008). Larvae were anesthetized, paralyzed, and then bathed in extracellular solution during the experiments. Patch electrodes were pulled to 5- to 8-MΩ resistances and filled with 125 mM K-gluconate, 2.5 mM $MgCl_2$, 10 mM EGTA, 10 mM HEPES buffer, and 4 mM Na_2ATP and adjusted to pH 7.3 with KOH. Electrodes were carefully advanced through the skin and into the posterior lateral line ganglion under constant positive pressure (~50 mmHg) with a pneumatic transducer to keep the tip from clogging. On breaking into the ganglion, an afferent cell was quickly targeted, and a gigaohm seal was achieved by equilibrating the electrode to atmosphere or by manually applying gentle suction. A holding potential of −65 mV was applied once the electrode became cell-attached and the membrane was punctured with manual suction pulses. Recordings were made with a MultiClamp 700B amplifier (Axon Instruments) at a gain of 20 [feedback resistor (rf) = 500 MΩ] filtered with a low-pass filter set at 30 kHz and digitized at 63 kHz.

Only cells that fired spontaneous action potentials with a resting membrane potential between −45 and −70 mV were included in our analysis. For each patched cell, input resistance measurements were calculated from an average of five hyperpolarizing square current pulses between 10 and 40 pA in the linear current-voltage range. Since afferents fire spontaneously, only current steps that did not intercept firing events were used to construct the current-voltage relationship

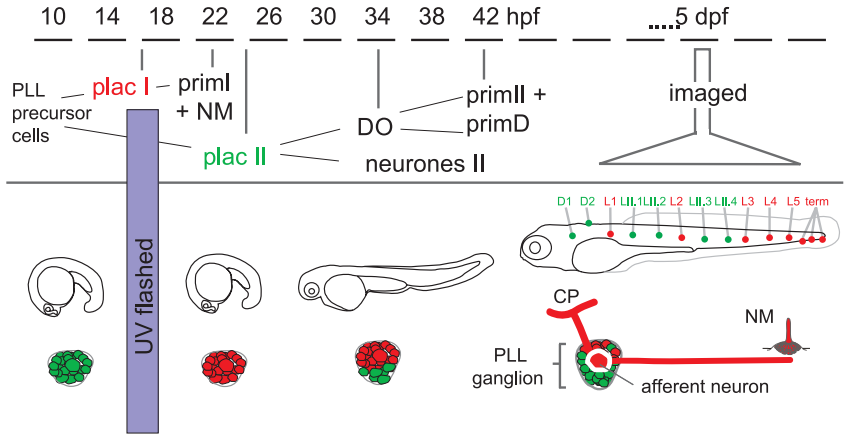

Fig. 1. Timeline of afferent neuron photoconversion in HuC:Kaede fish during the development of the posterior lateral line (PLL), with the timeline reproduced from Sarrazin et al. (2010) and used with permission from *The Journal of Neuroscience*. Initially, all afferent neurons are green. When larvae are exposed to UV light at 17 h postfertilization (hpf), all afferent neurons are converted to red. Neurons that subsequently develop after 17 hpf are green. Thus, when the lateral line ganglion is imaged at 5 days postfertilization (dpf), red signifies older cells, and green represents younger cells. Although neuromasts (NM) are not labeled by HuC:Kaede, here they are colored to symbolize the age of the placode that they are derived from. L and terminal neuromasts are derived from placode (plac) I, whereas LII and D neuromasts are derived from placode II. A single bipolar lateral line afferent neuron is highlighted to show the relationship of a presynaptic neuromast to the central projection (CP) into the hindbrain. Vertical gray bars indicate approximate timeline of development. DO is the group of cells from which primordium II (primII) and primD are derived, shown at 34 hpf (Sarrazin et al. 2010).

(*I-V*) curve. Additionally, in some cells, a hyperpolarizing holding current was applied once the electrode had become cell-attached to quiet the cell before we applied current steps to conduct our resistance measurements. We found no significant differences in resistance values between cells, so the data were pooled. To reveal the connectivity of patched cells to neuromasts in HuC:Kaede fish, the patch solution included 0.5% Alexa Fluor 647. After several minutes to ensure dye uptake, the number and location of neuromasts contacting the patched cell was confirmed with an integrating CCD camera and a Cy5 filter set with an epifluorescence light source.

Ventral root recordings of fictive motor behavior. We followed the hydrodynamic stimulation and ventral root recording response protocol from a previous study (Liao 2010), although note that we stimulated different neuromasts here. To confirm stimulation during ventral motor root recordings, we monitored patch recordings from connected afferent neurons and captured images of the cupula and apical hair bundles being deflected by the water jet with a high-speed video camera (1024- × 1024-pixel resolution at 250 frames per second; Phantom v12; Vision Research).

Labeling afferent neuron central projections and their postsynaptic hindbrain targets. Single neuromasts were backfilled to visualize the central projections of their afferent neurons onto hindbrain targets. We electroporated D2 and L5 neuromasts with rhodamine and Alexa Fluor 647, respectively, in the Vglut-GFP line to look for differences in postsynaptic candidates. In another set of experiments using wild-type larvae, we backfilled the Mauthner cell with Alexa Fluor 488 dextran (Molecular Probes) and D2 neuromasts with rhodamine dextran to confirm contacts onto the Mauthner cell. All fish were electroporated at 5 dpf, given 1 day to recover, and then imaged at 6 dpf with a confocal microscope.

Confocal imaging. Larvae were anesthetized and embedded in agar with their dorsal side against the glass bottom of a dish. To prevent desiccation of the preparation while imaging, a 0.02% solution of MS-222 in Hank's solution was placed on top of the agar. Images were collected with a Leica SP5 confocal microscope with a Leica HCX PL APO ×63/1.20-numerical aperture water-immersion objective and settings for tetramethylrhodamine isothiocyanate (TRITC)/FITC/Cy5 (494/518, 541/572, and 650/670 nm excitation/emission, respectively). To construct images of the glutamatergic hindbrain stripes, 1024- × 1024-pixel images were rotated and stacked. To look at putative contacts between the lateral line and hindbrain targets, images were taken along the dorsoventral axis of the body with a step size of 1 μm with 1024- × 1024-pixel resolution. Images were taken at high-gain settings and averaged to prevent photo damage.

Analysis. I-V and neuronal activity were recorded with pClamp v9.2, analyzed offline with DataView (Dr. William Heitler, University of St. Andrews) to measure input resistance and spontaneous firing frequency, and plotted in MATLAB v7.0. The spontaneously firing frequency was then plotted as a function of the cross-sectional area of the cell, which was calculated with Image-Pro v5.0 (Media Cybernetics) from the digitized circumference of a cell at its largest cross-section using Nomarski optics. For fictive behavior experiments, the relative intensity of each motor response was calculated as the mean, rectified spike amplitude normalized by the peak spike amplitude observed for the behavior, as previously calculated (Liao 2004). All values are reported as the means ± SE.

We chose an arbitrary reference point to quantify the position of the L5 and D2 hindbrain projections relative to the lateral dendrite of the Mauthner cell. We imported *z*-stacks of confocal images into ImageJ [v1.43u; National Institutes of Health (NIH)], created a *z*-projection, and selected an area of interest for analysis (70 × 25 μm). To minimize the contribution of background noise for each projection, we measured the grayscale value in a region devoid of the structures of interest and subtracted this value from the grayscale values of each structure. We then normalized these noise-corrected values to their respective peak values for each of the color channels. Data from five fish were averaged, and the SE of the mean was reported. A cutoff value of 1 SD was also applied to illustrate better the areas of strongest signal.

RESULTS

Afferent neuron age, size, and connectivity to neuromasts. We labeled individual afferent neurons in the posterior lateral line ganglion of flashed, HuC:Kaede fish. Older afferent neurons were found in the central and dorsal region of the ganglion, whereas younger afferent neurons were located in the peripheral and ventral region. Forty-three cells were labeled, their cross-sectional areas recorded, and their axonal projections traced to specific neuromasts along the body. Thirty cells were labeled by single-cell electroporation and the remaining 13 by patch recordings. We found that cell area varied, ranging from 27.3 to 172.3 μm^2 with an average of 83.6 ± 6.1 μm^2 (mean ± SE). The area of an afferent cell was correlated to its age. Older cells were significantly larger (Fig. 2*A*; 90.4 ± 13.7 μm^2) than younger cells (Fig. 2*B*; 63.5 ± 5.8 μm^2; Student's *t*-test, $P < 0.05$). More than half of the afferent neurons (65%) contacted a single neuromast, and, of these, the majority (79%) consisted of younger cells (Fig. 2*C*). Younger cells tended to contact neuromasts that were located closer to the head, although they could contact neuromasts located throughout the body. A smaller percentage of cells (21%) contacted two neuromasts, the majority (67%) of which consisted of older cells. Only older cells contacted 3 or more neuromasts, which often included a terminal neuromast located at the tail. Afferent neurons that contacted one terminal neuromast typically contacted other terminal neuromasts but could also contact other neuromasts along the body. Afferent neurons were not limited to contacting neuromasts derived from the same primordium. Thus older cells derived from primordium I could contact a neuromast derived from primordium II (e.g., LII neuromasts), and younger cells derived from primordium II could contact a neuromast derived from primordium I. We did not find an older cell that contacted only a single, terminal neuromast. We did not find a younger cell that contacted >1 D neuromasts.

A one-way ANOVA was used to test whether the cell area had an effect on the caudal-most location of a neuromast that it contacts. Cell area differed according to the body location of the neuromast that it contacted, $F(11, 31) = 8.3$, $P = 1.4 \times 10^{-6}$. Bonferroni post hoc tests indicate that younger cells that innervate anterior neuromasts are generally smaller than afferents that innervate more posterior neuromasts ($P < 0.05$). For example, an afferent cell that innervated D2 was smaller than an afferent cell that innervated the terminal neuromasts.

Physiological correlates to cell size. Afferent neurons show spontaneous spiking activity due to the constant release of glutamate from the hair cells of the neuromasts (Trapani and Nicolson 2011). We performed whole cell patch-clamp recordings for different-sized afferent neurons (Fig. 3, *A* and *B*) and recorded input resistance and spontaneous spiking rate in both 5-dpf wild-type and HuC:Kaede fish. Values did not differ significantly between the two groups of fish so the data were pooled (Student's *t*-test, $P > 0.05$). Our recordings revealed that afferent neurons possessed excitable soma that could generate tonic firing in response to depolarizing current steps, both in the presence of spontaneous activity as well as when the cell was quieted by hyperpolarization (Fig. 3, *C* and *D*).

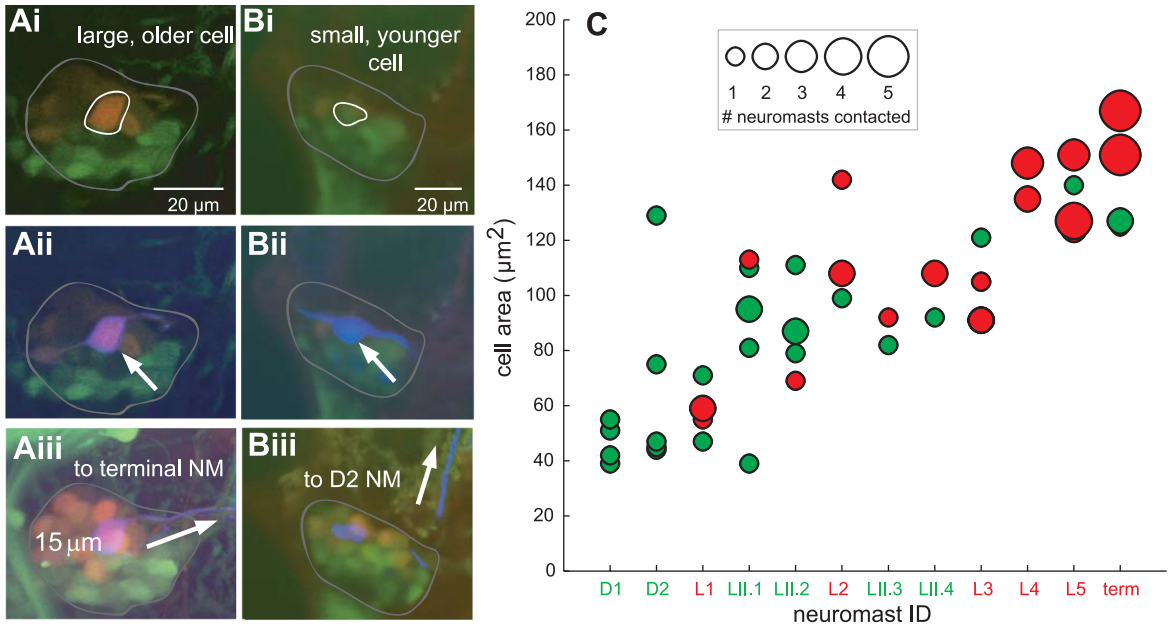

Fig. 2. Older (red) and younger (green) afferent neurons in HuC:Kaede larvae can be individually labeled (blue) to reveal differences in the location and number of neuromasts innervated. *Ai*: a large, older cell (white outline) is targeted for labeling in the ganglion (gray outline). On successful electroporation, the cell is double-labeled (*Aii*; arrow). A merged image reveals a projection coursing down the body toward the terminal neuromasts of the tail (*Aiii*; arrow). *Bi*: a small, younger cell is targeted for labeling. *Bii*: the successfully electroporated cell is double-labeled. A merged image reveals a projection that rises sharply toward the D2 neuromast (*Biii*; arrow). Dorsal is the *top* of the image, and anterior is to the *left*. *C*: plot of afferent somata size against the number and location of the neuromast(s) that it innervates. The size of the data symbol represents the number of neuromasts innervated, and the location of the data symbol along the *x*-axis indicates the most caudal neuromast innervated. Large, older afferents contact more neuromasts, of which the most caudal tended to be located closer to the tail compared with the neuromasts contacted by smaller, younger afferents. Neuromasts on the *x*-axis label are color-coded to symbolize the placode from which they were derived. Red indicates a neuromast derived from placode I, and green indicates a neuromast derived from placode II. A discrepancy between afferent neuron and neuromast color indicates that cells are not restricted to contacting neuromasts derived from the same placode.

Although cells displayed a continuum of sizes, we generally found that cells that had an area smaller than ~50 μm^2 had a higher spontaneous firing frequency and were more excitable than cells larger than ~100 μm^2 (Fig. 3, *E* and *F*). Spontaneous spike frequency ranged from about 5 to 50 Hz. There is a significant linear relationship between cell size and spike frequency (Fig. 3*G*; $r^2 = 0.53$, $P < 0.05$). We found that a wide range of cell sizes fired spontaneously at <15 Hz, whereas only smaller cells fired at frequencies >30 Hz. Larger cells were restricted to lower spontaneous spike frequencies than smaller cells. There is a significant linear relationship between cell size and input resistance (Fig. 3*H*; $r^2 = 0.79$, $P < 0.05$), whereby smaller cells had a higher resistance than larger cells.

Fictive motor responses to hydrodynamic stimulation of single neuromasts. Careful stimulation of a single terminal neuromast with a controlled water jet (~2 cm/s) showed that tail neuromasts play an important role in generating motor responses such as swimming and escapes (Fig. 4*A*; $n = 7$ fish). Ventral root recordings revealed that stimulation of terminal neuromasts elicited relatively fast (37.6 ± 14.2 Hz) vs. slow (lower than ~25 Hz) swimming frequencies (Liao and Fetcho 2008). In contrast, there were fewer motor responses when the D2 neuromast was stimulated (as measured by the normalized, rectified signal; see METHODS), which is generally contacted by younger afferent neurons (Fig. 4, *C* and *D*; Student's *t*-test, $P < 0.05$). We recorded from afferent neurons contacting the terminal and D2 neuromasts to verify stimulation even in the absence of a motor response. We showed that spike frequency increases in afferent neurons as a response to neuromast stimulation. However, there was no correlation between stimulated spike frequency and soma area for afferent neurons that contacted D2 or terminal neuromasts ($y = 0.12x + 183.78$, $r^2 = 0.06$, $P = 0.46$; Fig. 4*E*). We found no difference between the firing frequencies of afferent neurons associated with the D2 (194.6 ± 87.0 Hz) and terminal (197.0 ± 74.5 Hz) neuromasts (Student's *t*-test, $P < 0.05$).

Hindbrain targets of afferent neuron central projections. We used the Vglut-GFP line to trace where afferent projections mapped onto hindbrain regions (Fig. 5, *A–C*) with a recently described functional organization (Kinkhabwala et al. 2010). We discovered that the afferent projections terminated onto the lateral-most glutamatergic hindbrain stripe in all of the individuals that we looked at ($n = 11$ fish). This region corresponds to an area known as the medial octavolateralis nucleus (MON). Although there are putative contacts onto glutamatergic neuropil (Fig. 5, *D–F*), there are no obvious contacts onto glutamatergic cell bodies. Afferents connected to neuromasts closer to the tail (i.e., L5) contact dorsal neuropil in the MON, whereas afferents connected to neuromasts closer to the head (i.e., D2) contact ventral neuropil (Fig. 5*B*). The L5 neuromast made contact with the lateral dendrite of the Mauthner cell (Fig. 5, *G–I*), a large neuron that initiates the escape response (Hatta and Korn 1999). We looked at five individuals and found that afferent projections from L5 neuromasts projected more medially than D2 neuromasts, closer to the lateral dendrite of the Mauthner cell (Fig. 5, *Ji* and *Jii*).

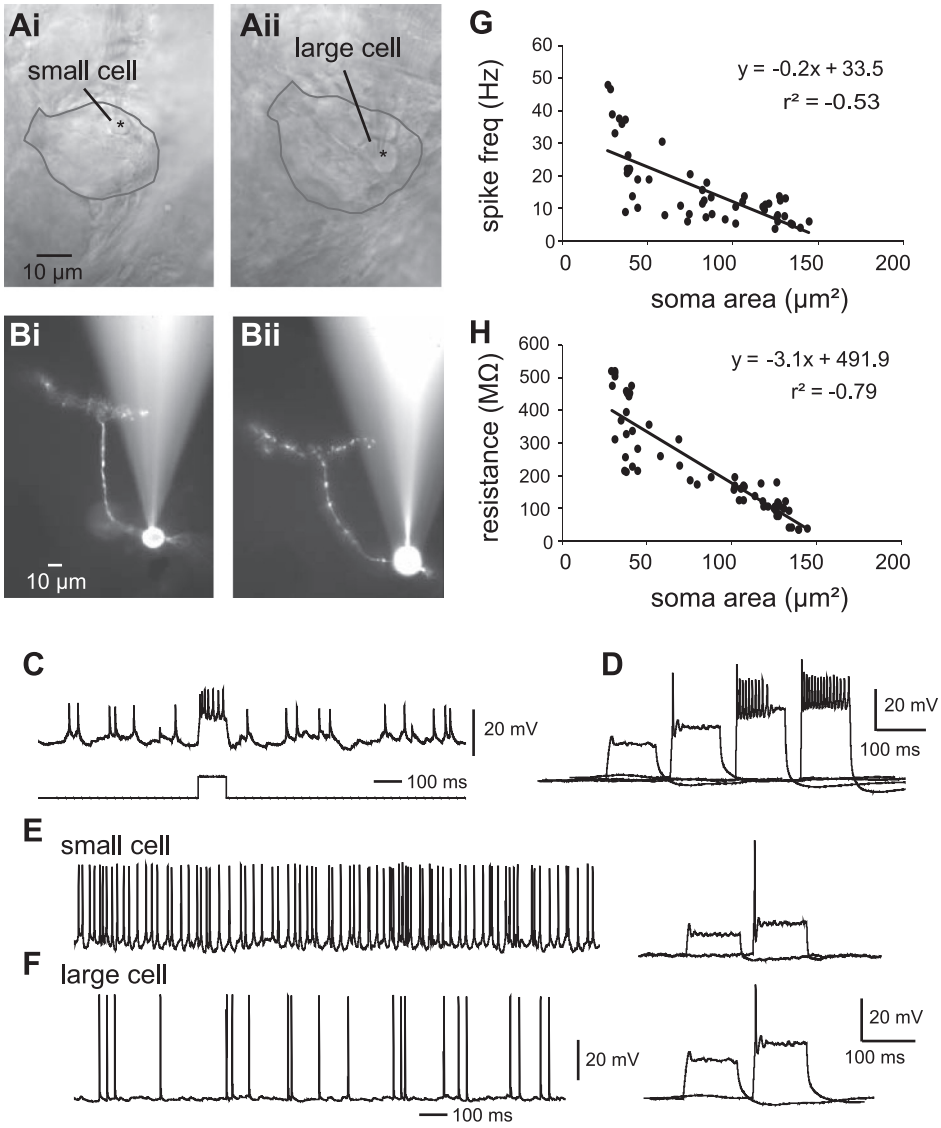

Fig. 3. Whole cell patch-clamp recordings of afferent neurons reveal differences in physiology with cell size. *Ai* and *Aii*: both small and large cells in the ganglion can be targeted for recording with Nomarski optics. *Bi* and *Bii*: after a successful recording, the cell body and its projections to the neuromasts and hindbrain are revealed under a fluorescence microscope. *C*: afferent neurons are spontaneously active and increase their firing rate on depolarization by current injection. *D*: increasing current injection steps elicit tonic firing even in the absence of background spontaneous firing when the cell is hyperpolarized. *E*: smaller cells have a higher spontaneous spike frequency and lower rheobase than larger cells (*F*). *G*: there is an inverse relationship between soma area and spontaneous spike frequency (freq; $n = 53$). *H*: there is an inverse relationship between soma area and input resistance ($n = 62$).

DISCUSSION

There is a large body of literature that characterizes the lateral line system for adult fishes. Several anatomic studies provide great detail in tracing lateral line central projections into the brain (references within McCormick 1989). However, most studies lack the resolution to reveal individual neuromast connections into the hindbrain, for which the larval zebrafish system is more appropriate. In adult fishes, the lateral line projects to at least four different brain regions: *1*) the MON; *2*) the Mauthner neuron; *3*) the caudal nucleus; and *4*) the eminentia granularis in the cerebellum (McCormick 1989). We believe that in 5-dpf larvae, the central projections of the posterior lateral line are likely located in at least three of these regions, which demonstrates the functional importance of these connections at an early life history stage (Mueller and Wullimann 2005). Using the otic capsule as a shared landmark, we determined that lateral line projections that terminate in the lateral-most glutamatergic stripe contact the eminentia granularis, MON, and the Mauthner neurons. We are less certain of the contact to the caudal nucleus but cannot rule it out. Translating larvae brain structures to their better known adult counterparts can be challenging. For example, rhombic lip-derived structures such as the cerebellum arise relatively late in development compared with other structures, such as the optic tectum. Although the MON in adults is directly ventral to the cerebellar crest neuropil, which is a caudal extension of the cerebellum, this relationship is less clear in young larvae. A future study that shows which regions of the larval brain correspond to regions in the adult zebrafish would be invaluable, given that *1*) the larval brain is rapidly developing so the connections and regions they contact may be different when examined in adults, and *2*) substantial differences in contact regions have been shown to exist across species in adults.

Our physiological recordings provide the first functional interpretation of lateral line somatotopy in larval zebrafish (Alexandre and Ghysen 1999; Fame et al. 2006; Gompel et al. 2001). When our data are taken together with previous work (Gompel et al. 2001; Pujol-Marti et al. 2010), it is clear that the intrinsic properties and projection patterns of afferent neurons match their birth date. These authors found that older neurons are associated with caudal neuromasts and project more dorsally into the hindbrain. We found that the first developing neurons not only share these connection targets, but also have the largest soma at *day 5*, which, along with their larger axon

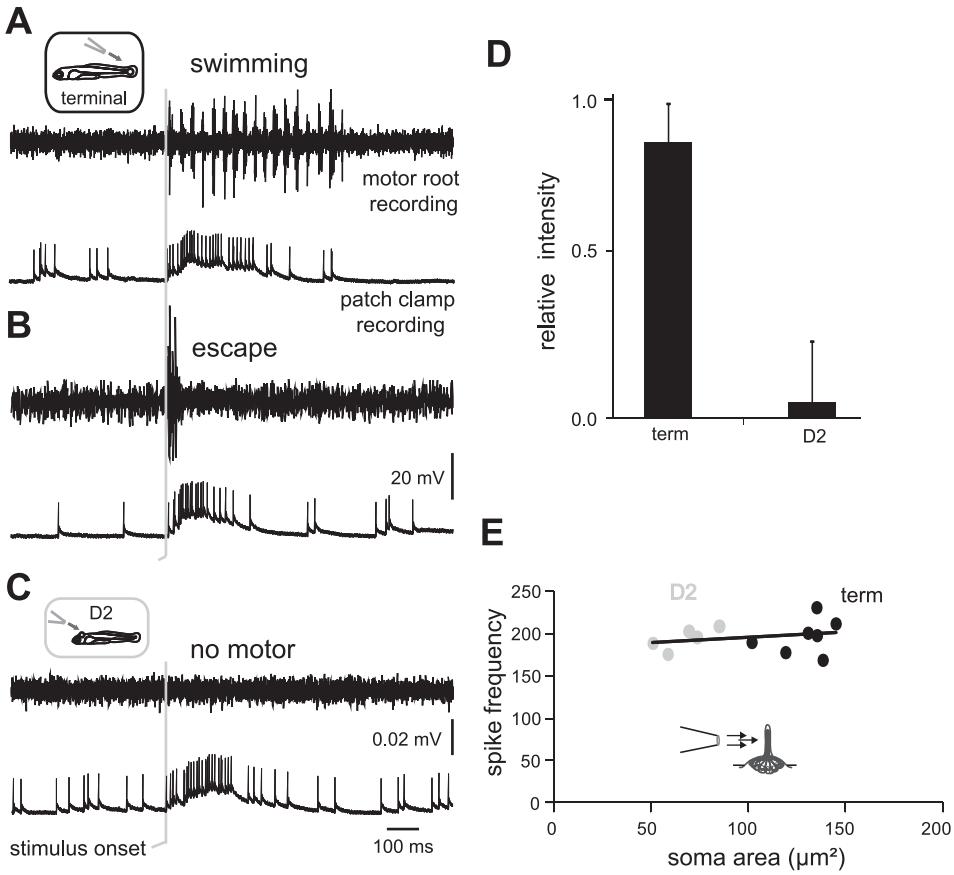

Fig. 4. Stimulation of a terminal, but not D2, neuromast reliably initiates a motor response. A water jet directed at a terminal neuromast causes the connected afferent neuron to fire and elicits either a swimming (*A*) or escape (*B*) response in a fictive preparation. *C*: the same water jet stimulates the D2 neuromast but does not elicit a reliable motor response. *D*: across individuals, there is more motor activity when a terminal neuromast is stimulated compared with a D2 neuromast (mean ± SE; Student's *t*-test, $P < 0.05$; $n = 4$ fish). *E*: a water jet to D2 and terminal neuromasts elicits no difference in afferent neuron spike frequency, suggesting that different projections into the hindbrain rather than spiking activity causes the distinct motor responses observed.

diameters (Schellart and Kroese 2002) and longer projections that branch onto multiple neuromasts, cause them to have a lower input resistance than later-born cells. These older cells are less excitable and have a lower spontaneous firing rate, placing them in a unique position to register stronger flow stimuli such as those generated from a predator (McHenry et al. 2009). In contrast, subsequently developing afferents are smaller at *day 5*, have a higher spontaneous firing rate, can possess a lower firing threshold, and are more inclined to contact single neuromasts (Nagiel et al. 2008). Younger afferents are therefore more excitable and may be better suited for detecting weaker flow stimuli in localized regions of the body, maturing perhaps to coincide with the onset of feeding and prey detection. We envision that an initial, broad sensory scaffold is established by afferents and neuromasts derived from placode I to detect coarse flow, followed by a second wave of cells derived from placode II that would confer the ability to detect flow with greater sensitivity and finer spatial resolution. This architecture would separate different types of flow information at the periphery and likely ease the task of processing inputs at higher-order brain centers such as the torus semicircularis (New et al. 1996; Plachta et al. 2003).

Age-related function is a broad unifying principle of neuronal organization. In the spinal cord, large motor neurons and interneurons responsible for powerful movements develop first and smaller motor neurons and interneurons develop later to facilitate finer motor control (Bhatt et al. 2007; Cope and Sokoloff 1999; McLean et al. 2007). Recently, this blueprint has been extended into the hindbrain, where neurons form distinct stripes with overlapping neurotransmitter and transcription factor phenotypes. These neurons are spatially assembled according to the strength of an associated motor behavior (Kinkhabwala et al. 2010; Koyama et al. 2010). For example, in the medial-most glutamatergic stripe, the dorsal neuropil is contacted by older, ventral neurons that are responsible for generating powerful movements such as fast swimming and the escape response. We believe that the afferent-to-neuromast organization reported here could also be related to the neuronal stripe organization in the hindbrain. As in the medial glutamatergic stripe, the dorsal neuropil in the lateral-most glutamatergic stripe is also contacted by older cells, which in our case turn out to be afferent neurons that are connected to tail neuromasts (Fig. 5*B*). We reason that if the functional pattern established in the medial glutamate stripe turns out to remain consistent in the lateral stripe, then the dorsal hindbrain projections of tail neuromasts would be favorably positioned to inform fast motor behaviors quickly, leaving the projections of rostral neuromasts to direct slower motor behaviors. The ascending inputs of the lateral line have been documented to make extensive contacts to various regions of the brain. The MON is the first processing stage in an ascending lemniscal pathway that includes additional processing stages in the midbrain (torus semicircularis and optic tectum) and forebrain (McCormick 1989). There is also a direct, local connection between the lateral line and the Mauthner cell that confers an ability to translate flow magnitude and direction into appropriate escape behaviors (Hatta and Korn 1999). The critically important speed of the Mauthner escape response has been shown to benefit from fewer processing stages involving both the anterior (Mirjany and Faber 2011) and posterior (Faber and

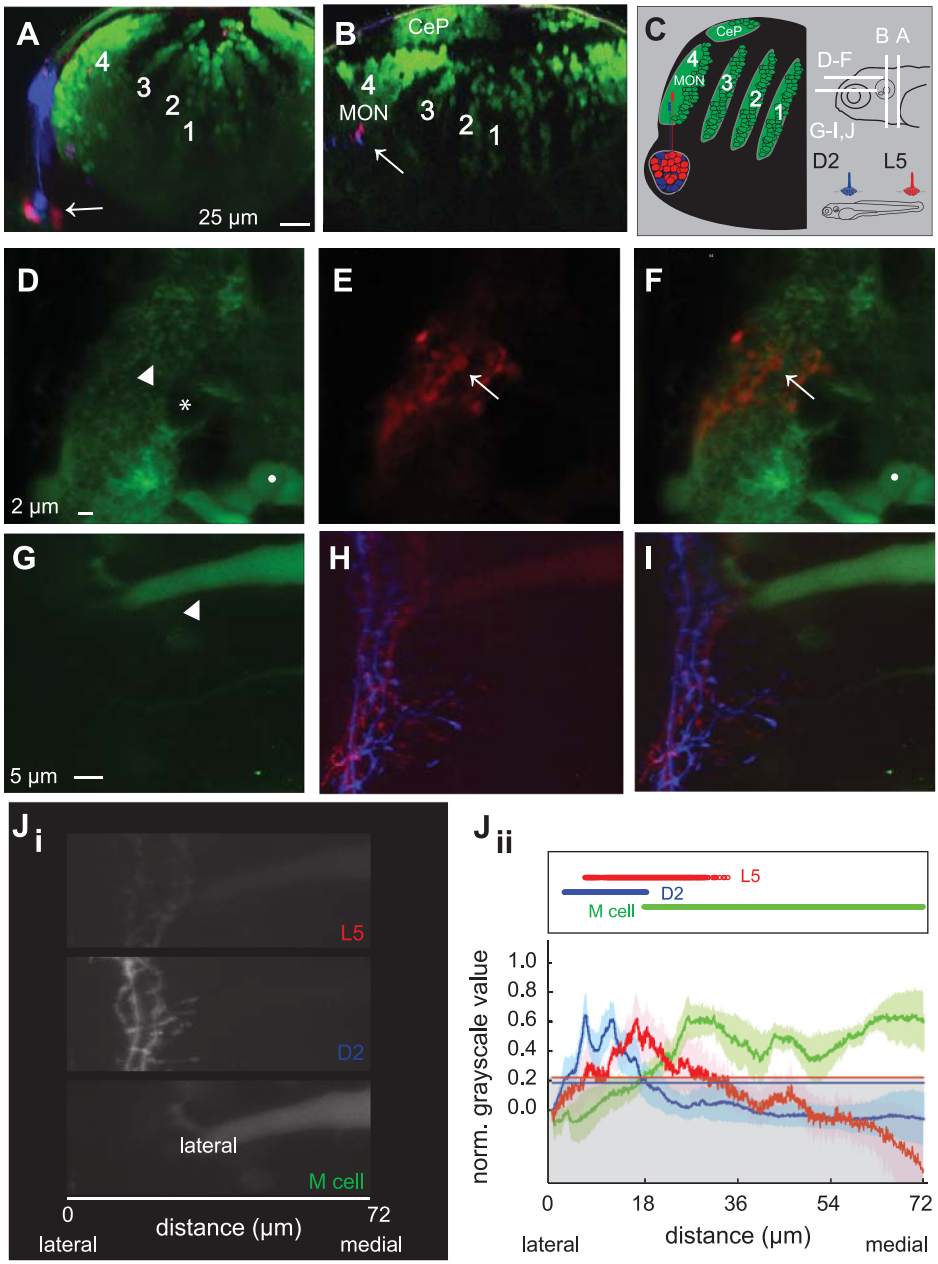

Fig. 5. Central projections of afferent neurons contact identified postsynaptic targets in the hindbrain. *A*: backfilled afferent soma (arrow) connected to a D2 (blue) and L5 (red) neuromast in a Vglut-GFP transgenic fish showing 4 glutamatergic stripes (green, numbered) in ½ of the hindbrain seen in cross-section (Kinkhabwala et al. 2010). *B*: a more rostral cross-section shows that afferent projections (arrow) of the L5 neuromast projects more dorsally onto the neuropil of the 4th, lateral-most glutamatergic stripe than afferents associated with the D2 neuromast. This region corresponds to the medial octavolateralis nucleus (MON) and lies ventral to the cerebellar plate (CeP). *C*: schematic stack of images between *A* and *B*, showing the D2 and L5 associated afferent neurons in the posterior lateral line ganglion (peripheral nervous system) with their hindbrain projections superimposed onto the 4th glutamatergic stripe that corresponds with the MON. Diagram of the head where cross-sectional images were taken. *D*: glutamatergic neuropil (arrowhead) and soma (dot) in the MON of a Vglut-GFP transgenic fish. A cell that is not labeled with green fluorescent protein (GFP) is evident, which is presumably not glutamatergic (asterisk). *E*: central projection terminals (arrow) of an afferent neuron connected to the L5 neuromast. *F*: merged image shows that terminals make putative contacts onto glutamatergic neuropil. *G*: the lateral dendrite of the Mauthner cell (green, arrowhead) was backfilled with Alexa Fluor 496 through the ventral spinal cord in a wild-type larvae and identified according to its characteristic size and morphology. *H*: central projection terminals of afferent neurons connected to the L5 neuromast (red) lie medial to those associated with the D2 neuromast (blue). Note that Alexa Fluor 496 is also moderately excited in the red channel. *I*: merged image of both afferent terminals show putative contacts with the lateral dendrite of the Mauthner cell. *Ji*: grayscale images illustrating the medial-lateral position of L5 and D2 afferent terminals relative to the Mauthner cell lateral dendrite. *Jii*: quantification of both D2 and L5 afferent terminals and the Mauthner cell lateral dendrite with respect to a reference point lateral to the afferent projections ($n = 5$ fish). Plot is for the structures shown in *Ji*, showing the SE around the mean values as well as the SD cutoff line for each structure. Higher grayscale values represent stronger signal. The area below the cutoff line has been grayed out, and the area above the cutoff line, which reveals the areas of strongest signal for each structure, is summarized in the *top* box. On average, L5 hindbrain terminals start and end more medially than D2 terminals and show more overlap with the Mauthner cell. Note that the SD cutoff line for the Mauthner cell is obscured by the cutoff line for the L5 projection. Background noise was subtracted from each channel before quantification. norm., Normalized.

Korn 1975) lateral line system (Eaton et al. 1977; Faber et al. 1989). Considering the physiology of afferent neurons and their pattern of contact onto hindbrain stripes, our results are consistent with the hypothesis that the posterior lateral line (L5)-MON circuit could circumvent higher-order processing centers to *1*) make fine adjustments to swimming speed, and *2*) provide another mechanism to initiate swimming in addition to the posterior lateral line (L5)-Mauthner cell circuit. We believe stimulation of terminal neuromasts can uniquely influence motor behaviors due to the intrinsic properties and hindbrain projections of their associated afferent neurons, given that there do not seem to be larger numbers of afferent representation for caudal neuromasts vs. more rostral neuromasts (Haehnel et al. 2012). In this way, selective stimulation of the larval lateral line may modulate a range of motor behaviors, from the onset of escape responses to the selection of swimming speed. Additionally, feedback from the lateral line may turn out to play a role in optimizing swimming performance by stabilizing inflected boundary layers, for which the terminal neuromasts are favorably positioned along the body (Anderson et al. 2001; Müller et al. 2000).

As zebrafish mature, it is likely that the simple organization present at the larval stage becomes obscured through differential patterns of growth and plasticity (Chiba et al. 1988; Fraser 1983; Gaze et al. 1974). For instance, afferent neurons could selectively change their synaptic strengths with their hair cell partners. This process has been shown to play a part in focusing an originally distributed set of connections, such as in the visual cortex and neuromuscular junction (Bennett and Pettigrew 1974, 1975; Brown et al. 1976; Hubel et al. 1977; Thompson 1985). In addition to the physiological heterogeneity between afferent neurons that may arise from intrinsic channel density and activity (Eatock et al. 2008; Sarrazin et al. 2010; Trapani and Nicolson 2011), this raises the possibility that, with age, synaptic rearrangement can change the contact strength of older cells onto multiple neuromasts. This would increase the functional complexity of the system beyond what is documented here in larvae. Although our results may turn out to be limited to early stages of development, we find it unlikely that this initial organization would be substantially rearranged at later stages of growth. We suggest that this initial scaffold is built on and elaborated, rather than dismantled and reconstructed, according to current challenges that the hydrodynamic environment poses on the organism as it matures. A promising future direction will therefore be to determine what portion of this organization is the result of developmental timing (e.g., small, younger afferent neurons will grow larger and synapse with more and more posterior neuromasts) vs. an established pattern that persists into the adult stage.

ACKNOWLEDGMENTS

We thank Joseph R. Fetcho for discussions that led to some of the experiments, the Vglut-transgenic line, and comments on an earlier version of the manuscript. Mario Wullimann kindly provided assistance on larval zebrafish brain anatomy. Masashige Taguchi helped perform some of the statistical analyses. Katherine Decesare and Christina Walker provided excellent care in maintaining and breeding fish. We thank Hitoshi Okamoto of the RIKEN Brain Science Institute and the support of National BioResource Project of Japan for generously supplying us with the Tg(HuC:Kaede)/rw0130a fish.

GRANTS

This work was supported by NIH Grants R01-NS-26539 (to Joseph R. Fetcho) and R01-DC-010809 (to J. C. Liao).

DISCLOSURES

No conflicts of interest, financial or otherwise, are declared by the author(s).

AUTHOR CONTRIBUTIONS

J.C.L. conception and design of research; J.C.L. and M.H. performed experiments; J.C.L. and M.H. analyzed data; J.C.L. interpreted results of experiments; J.C.L. and M.H. prepared figures; J.C.L. drafted manuscript; J.C.L. and M.H. edited and revised manuscript; J.C.L. and M.H. approved final version of manuscript.

REFERENCES

Alexandre D, Ghysen A. Somatotopy of the lateral line projection in larval zebrafish. *Proc Natl Acad Sci USA* 96: 7558–7562, 1999.

Anderson EJ, McGillis WR, Grosenbaugh MA. The boundary layer of swimming fish. *J Exp Biol* 204: 81–102, 2001.

Bae YK, Kani S, Shimizu T, Tanabe K, Nojima H, Kimura Y, Higashijima S, Hibi M. Anatomy of zebrafish cerebellum and screen for mutations affecting its development. *Dev Biol* 330: 406–426, 2009.

Bennett MR, Pettigrew AG. The formation of synapses in amphibian striated muscle during development. *J Physiol* 252: 203–239, 1975.

Bennett MR, Pettigrew AG. The formation of synapses in striated muscle during development. *J Physiol* 241: 515–545, 1974.

Bhatt DH, McLean DL, Hale ME, Fetcho JR. Grading movement strength by changes in firing intensity versus recruitment of spinal interneurons. *Neuron* 53: 91–102, 2007.

Brown MC, Jansen JK, Van Essen D. Polyneuronal innervation of skeletal muscle in new-born rats and its elimination during maturation. *J Physiol* 261: 387–422, 1976.

Chiba A, Shepherd D, Murphey RK. Synaptic rearrangement during postembryonic development in the cricket. *Science* 240: 901–905, 1988.

Coombs S, Gorner P, and Munz H. (editors). *The Mechanosensory Lateral Line: Neurobiology and Evolution*. New York: Springer-Verlag, 1989.

Coombs S, Mogdans J, Halstead M, Montgomery J. Transformation of peripheral inputs by the first-order lateral line brainstem nucleus. *J Comp Physiol A* 182: 606–626, 1998.

Cope TC, Sokoloff AJ. Orderly recruitment among motoneurons supplying different muscles. *J Physiol (Paris)* 93: 81–85, 1999.

Dijkgraaf S. The functioning and significance of the lateral-line organs. *Biol Rev Camb Philos Soc* 38: 51–105, 1963.

Eatock RA, Xue J, Kalluri R. Ion channels in mammalian vestibular afferents may set regularity of firing. *J Exp Biol* 211: 1764–1774, 2008.

Eaton RC, Bombardieri RA, Meyer DL The Mauthner-initiated startle response in teleost fish. *J Exp Biol* 66: 65–81, 1977.

Engelmann J, Hanke W, Bleckmann H. Lateral line reception in still- and running water. *J Comp Physiol A Neuroethol Sens Neural Behav Physiol* 188: 513–526, 2002.

Faber DS, Fetcho JR, Korn H. Neuronal networks underlying the escape response in goldfish. General implications for motor control. *Ann NY Acad Sci* 563: 11–33, 1989.

Faber DS, Korn H. Inputs from the posterior lateral line nerves upon the goldfish Mauthner cells. II. Evidence that the inhibitory components are mediated by interneurons of the recurrent collateral network. *Brain Res* 96: 349–356, 1975.

Fame RM, Brajon C, Ghysen A. Second-order projection from the posterior lateral line in the early zebrafish brain. *Neural Dev* 1: 4, 2006.

Faucherre A, Pujol-Marti J, Kawakami K, Lopez-Schier H. Afferent neurons of the zebrafish lateral line are strict selectors of hair-cell orientation. *PLoS One* 4: e4477, 2009.

Fraser SE. Fiber optic mapping of the *Xenopus* visual system: shift in the retinotectal projection during development. *Dev Biol* 95: 505–511, 1983.

Gaze RM, Keating MJ, Chung SH. The evolution of the retinotectal map during development in *Xenopus*. *Proc R Soc Lond B Biol Sci* 185: 301–330, 1974.

Gompel N, Dambly-Chaudiere C, Ghysen A. Neuronal differences prefigure somatotopy in the zebrafish lateral line. *Development* 128: 387–393, 2001.

Haehnel M, Taguchi M, Liao JC. Heterogeneity and dynamics of lateral line afferent innervation during development in zebrafish *(Danio rerio)*. *J Comp Neurol* 520: 1376–1386, 2012.

Hatta K, Korn H. Tonic inhibition alternates in paired neurons that set direction of fish escape reaction. *Proc Natl Acad Sci USA* 96: 12090–12095, 1999.

Hubel DH, Wiesel TN, LeVay S. Plasticity of ocular dominance columns in monkey striate cortex. *Philos Trans R Soc Lond B Biol Sci* 278: 377–409, 1977.

Kinkhabwala A, Riley M, Koyama M, Monen J, Satou C, Kimura Y, Higashijima S, Fetcho J. A structural and functional ground plan for neurons in the hindbrain of zebrafish. *Proc Natl Acad Sci USA* 108: 1164–1169, 2010.

Koyama M, Kinkhabwala A, Satou C, Higashijima S, Fetcho J. Mapping a sensory-motor network onto a structural and functional ground plan in the hindbrain. *Proc Natl Acad Sci USA* 108: 1170–1175, 2010.

Ledent V. Postembryonic development of the posterior lateral line in zebrafish. *Development* 129: 597–604, 2002.

Liao JC. Neuromuscular control of trout swimming in a vortex street: implications for energy economy during the Kármán gait. *J Exp Biol* 207: 3495–3506, 2004.

Liao JC. Organization and physiology of posterior lateral line afferent neurons in larval zebrafish. *Biol Lett* 6: 402–405, 2010.

Liao JC, Fetcho JR. Shared versus specialized glycinergic spinal interneurons in axial motor circuits of larval zebrafish. *J Neurosci* 28: 12982–12992, 2008.

McCormick CA. *Central Lateral Line Mechanosensory Pathways in Bony Fish*. New York: Springer-Verlag, 1989.

McHenry MJ, Feitl KE, Strother JA, Van Trump WJ. Larval zebrafish rapidly sense the water flow of a predator's strike. *Biol Lett*: 477–479, 2009.

McLean DL, Fan J, Higashijima S, Hale ME, Fetcho JR. A topographic map of recruitment in spinal cord. *Nature* 446: 71–75, 2007.

Mirjany M, Faber DS. Characteristics of the anterior lateral line nerve input to the Mauthner cell. *J Exp Biol* 214: 3368–3377, 2011.

Montgomery J, Bodznick D, Halstead M. Hindbrain signal processing in the lateral line system of the dwarf scorpionfish *Scopeana papillosus*. *J Exp Biol* 199: 893–899, 1996.

Montgomery J, Carton G, Voigt R, Baker C, Diebel C. Sensory processing of water currents by fishes. *Philos Trans R Soc Lond B Biol Sci* 355: 1325–1327, 2000.

Mueller T, Wullimann MF. *Atlas of Early Zebrafish Brain Development: A Tool for Molecular Neurogenetics* (1st ed.). Amsterdam: Elsevier, 2005.

Müller UK, Stamhuis EJ, Videler JJ. Hydrodynamics of unsteady fish swimming and the effects of body size: comparing the flow fields of fish larvae and adults. *J Exp Biol* 203: 193–206, 2000.

Nagiel A, Andor-Ardo D, Hudspeth AJ. Specificity of afferent synapses onto plane-polarized hair cells in the posterior lateral line of the zebrafish. *J Neurosci* 28: 8442–8453, 2008.

New JG, Coombs S, McCormick CA, Oshel PE. Cytoarchitecture of the medial octavolateralis nucleus in the goldfish, *Carassius auratus*. *J Comp Neurol* 366: 534–546, 1996.

Nicolson T, Rusch A, Friedrich RW, Granato M, Ruppersberg JP, Nusslein-Volhard C. Genetic analysis of vertebrate sensory hair cell mechanosensation: the zebrafish circler mutants. *Neuron* 20: 271–283, 1998.

Plachta DT, Hanke W, Bleckmann H. A hydrodynamic topographic map in the midbrain of goldfish *Carassius auratus*. *J Exp Biol* 206: 3479–3486, 2003.

Pujol-Marti J, Baudoin JP, Faucherre A, Kawakami K, Lopez-Schier H. Progressive neurogenesis defines lateralis somatotopy. *Dev Dyn* 239: 1919–1930, 2010.

Raible DW, Kruse GJ. Organization of the lateral line system in embryonic zebrafish. *J Comp Neurol* 421: 189–198, 2000.

Sarrazin AF, Nunez VA, Sapede D, Tassin V, Dambly-Chaudiere C, Ghysen A. Origin and early development of the posterior lateral line system in zebrafish. *J Neurosci* 30: 8234–8244, 2010.

Sato A, Koshida S, Takeda H. Single-cell analysis of somatotopic map formation in the zebrafish lateral line system. *Dev Dyn* 239: 2058–2065, 2010.

Sato T, Takahoko M, Okamoto H. HuC:Kaede, a useful tool to label neural morphologies in networks in vivo. *Genesis* 44: 136–142, 2006.

Schellart NA, Kroese AB. Conduction velocity compensation for afferent fiber length in the trunk lateral line of the trout. *J Comp Physiol A Neuroethol Sens Neural Behav Physiol* 188: 561–576, 2002.

Thompson WJ. Activity and synapse elimination at the neuromuscular junction. *Cell Mol Neurobiol* 5: 167–182, 1985.

Trapani JG, Nicolson T. Mechanism of spontaneous activity in afferent neurons of the zebrafish lateral-line organ. *J Neurosci* 31: 1614–1623, 2011.